07

Silicon differential photodetectors. Technology, characteristics, application

© V.V. Gavrushko, A.S. Ionov, O.R. Kadriev, V.A. Lastkin

Yaroslav-the-Wise Novgorod State University,
173003 Veliky Novgorod, Russia
e-mail: Valery.Gavrushko@novsu.ru

Received March 31, 2023
Revised June 8, 2023
Accepted July 3, 2023

A silicon-based photodetector containing two identical n^+-p-photodiodes is described. One of the photodiodes had a wide spectral response with high sensitivity in the ultraviolet region. The sensitivity of the second was reduced in the short-wavelength part of the spectrum by creating additional recombination centers in the near-surface region by implanting As ions. The spectral sensitivity of the differential signal obtained by subtracting photocurrents had a pronounced short-wavelength characteristic. The long-wavelength limit of the spectral range in terms of the $\lambda_{0.5}$ level, depending on the doping dose, was in the range of $0.37-0.47\,\mu$m. The sensitivity maximum corresponded to $\lambda_{\max} = 0.32-0.37\,\mu$m. The electrical and noise characteristics of the photodetector are given. The possibility of using differential photodetectors as two-color ones is shown.

Keywords: Photodiode, implantation, differential signal, ultraviolet, two-spectrum photodetector.

DOI: 10.61011/TP.2023.09.57366.136o-23

Introduction

In microelectronic measuring transducers, along with traditional ones, difference or differential methods [1,2] based on the registration of the difference between two signals are widely used. An example of the use of such techniques in optoelectronics is the use of differential amplifiers in coordinate-dependent photodetectors [3]. Difference signals are used in helio-trackers to orient the photovoltaic modules to maximize the solar flux [4]. To correct the inhomogeneity of matrix photosensitive elements, the most widely used scheme is based on comparing the signals of all (FFE) with two reference levels at uniform irradiation of the matrix [5]. The counter-acting thermistors ensure the stability of the bolometer performance [6]. In the present work, the possibility of using differential technology to correct the spectral response of silicon photodetectors is considered.

Silicon-based photodetectors both at present and in the near future will have wide applications in optoelectronics [7–10]. This is due to the highly developed and low-cost technology of silicon devices, as well as the ability to efficiently record optical radiation over a wide spectral range — from ultraviolet to infrared. In many cases, the radiation of observed objects has a limited spectral range, and it is reasonable to match it and narrow the spectral response of the photodetector [11], which will eliminate the influence of interfering objects with a different spectrum of radiation. Optical in-line filters [12–14] are commonly used to correct spectral sensitivity. The use of high quality external filters for deep stray radiation suppression can significantly increase the cost of devices [15] and is not always technically efficient. In addition, researchers have noted degradation of the devices due to the tendency of many light filters to solarize, especially for UV [16] radiation. Semiconductor filters are the most technologically advanced and stable, but they are only used to suppress sensitivity in the short-wave part of the spectrum [17]. The use of interference coatings [18–19] to highlight the short-wave area is not without disadvantages due to the dependence of characteristics on the angle of incidence of light on the filter surface and the difficulty of applying a large number of layers of strictly controlled thickness. The possibility of reducing sensitivity in the long-wavelength area by forming an inbuilt inhibitory field [20] also has limited effect. An interesting way to form the spectral sensitivity of a photodetector in the UV area by subtracting the signals of nearby sensitive sites with different spectral characteristics (differential photodetectors) [21–23]. As it turned out, such photodetectors have a number of specific features. In the present work, we describe a method for the preparation of silicon-based differential photodetectors using spectral sensitivity correction by implantation of heavy As [24] ions. The peculiarities of their characteristics established by the authors are given. Methods of controlling the range of spectral sensitivity are analyzed, examples of possible use of such photodetectors are given.

1. Structure and technology of photodetector

The structure of the proposed photodetector is shown in Fig. 1.

The photodetector contained two sites whose spectral sensitivities were identical in the long wavelength area but

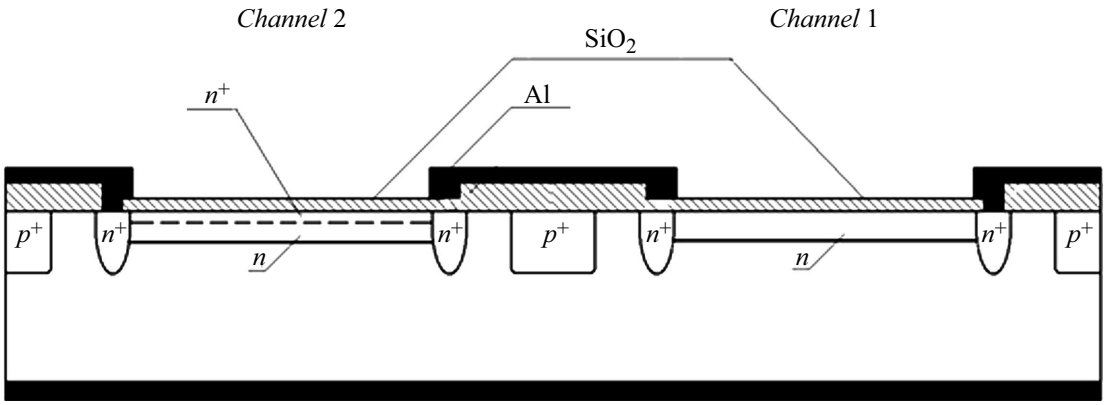

Figure 1. Structure of a differential photodetector

different for UV radiation. The first (main) channel was formed as a photodiode with a shallow $p-n$-junction [25,26] to ensure sensitivity in the broad spectral area. The starting material was p-type silicon of grade KDB-10. The electron-hole transition was created by implantation of phosphorus ions with a dose of $3\,\mu$C/cm^2 at an energy of 100 keV followed by thermal Annealing. The final depth of the $p-n$-transition, determined by the spherical slip method, was $1.1\,\mu$m. To ensure ohmic contact with the n -layer, additional sub-contact doping was performed along the peripheral region of the photosensitive layer by phosphorus implantation with a dose of $100\,\mu$C/cm^2. To limit the inversion channels introduced by the oxide charge, diffusion p^+-regions were formed. In order to reduce the reflection coefficient of incident radiation, an anti-reflection film SiO_2 with a thickness of about 60 nm and optimized for a wavelength of 350 nm was grown on the photosensitive region. Ohmic contacts were obtained by sputtering aluminium followed by annealing at 450°C. The aluminium films also acted as an optical screen, setting the dimensions of the photosensitive pads. In order to reduce the coupling between the channels, the minimum screen size was chosen to be 5–6 times larger than the diffusion length of non-main charge carriers [27,28].

The second (additional) channel was formed simultaneously with the first on the same wafer using common technological operations, but with the addition of a high dose of arsenic at the final stages of the implantation process. Implantation was performed at an energy of 50 keV in the dose range of 200 to $5000\,\mu$C/cm^2 without subsequent thermal annealing. The ion-doped layer created structural defects, which led to an increase in the recombination rate of photo-carriers formed by UV [29] radiation. In addition, the impurity inhibition profile during implantation [30–32] could create an inhibitory electric field for light-generated non-basic charge carriers in the near-surface area. Thus, the presence of the ion-doped layer reduced the sensitivity of the photodiode in the UV range due to both recombination processes and the creation of an inhibitory electric field. At the same time, the identity

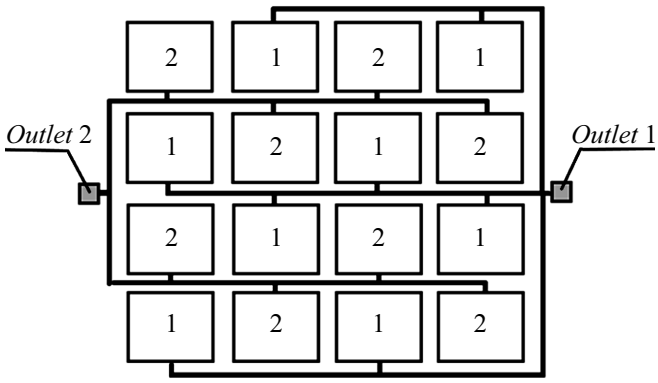

Figure 2. Location topology of the main (*1*) and auxiliary (*2*) photodetector channels.

of the deep layers provided close spectral sensitivity in the long-wavelength area, where the photocarrier collection processes were determined by areas distant from the surface. The size of the receiving sites for both channels was the same.

To reduce the influence of the inhomogeneity of the physical characteristics of the structure as well as the non-uniformity of the light flux on the spectral response, we proposed to form the channels in the form of two groups of parallel switched photodiodes. The photodiodes of the first and second channels were staggered as shown in Fig. 2. The total size of the photosensitive area was 2.5×2.5 mm.

Attempting to predict quantitative physical characteristics of such a photodetector using mathematical modelling, such as spectral sensitivity, is challenging. This is due to problems in determining the values of structural defect concentration, their distribution, parameters of recombination centers, especially since these values are subject to changes in multi-stage technological operations. In this connection, it was expedient to carry out an experimental study of the characteristics of such devices in order to obtain reliable information.

2. Spectral characteristics of photodetectors

Fig. 3 shows as an example the spectral sensitivity for an equal flux of incident quanta in relative units for channel *1* and channel *2* subjected to additional arsenic implantation with an energy of 50 keV and a dose $2000\,\mu C/cm^2$. The measurements were carried out in the photocurrent registration mode close to the short-circuit mode. As can be seen, the introduction of additional recombination centers allowed to reduce the sensitivity of the second channel in the UV area by an order of magnitude. At the same time, when shifting to the visible area, the difference between the signals in both channels decreased. Fig. 4 shows the spectral response at the output of a differential amplifier (let's call it a differential channel) obtained by subtracting the photocurrents of the main and auxiliary channels.

The characterization had a pronounced maximum in the UV area around $0.35\,\mu$ m. The limits of the spectral range in level $\lambda_{0.5}$ were within $0.27-0.46\,\mu$ m. The sensitivity of the differential channel for longer wavelengths ($\lambda > 0.7\,\mu$m) was reduced by almost two orders.

One of the significant factors determining the type of spectral characteristic of the differential channel was the

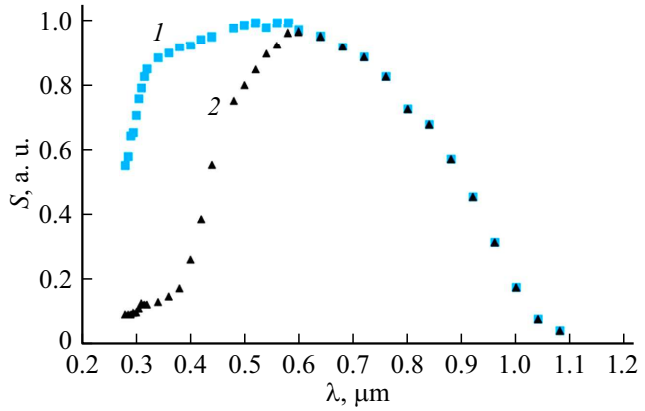

Figure 3. Spectral sensitivity of the main (*1*) and auxiliary (*2*) channels.

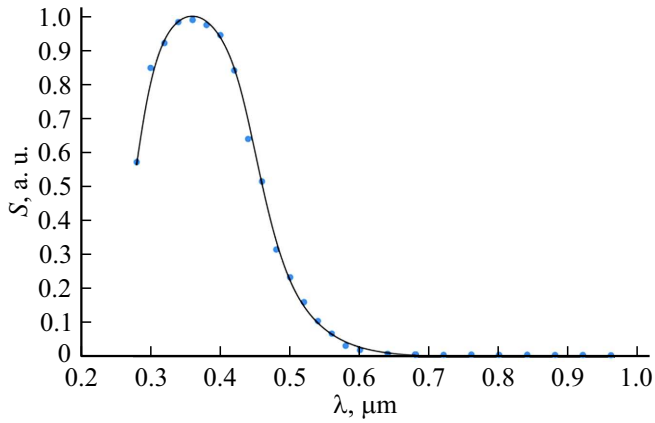

Figure 4. Spectral sensitivity of the differential channel

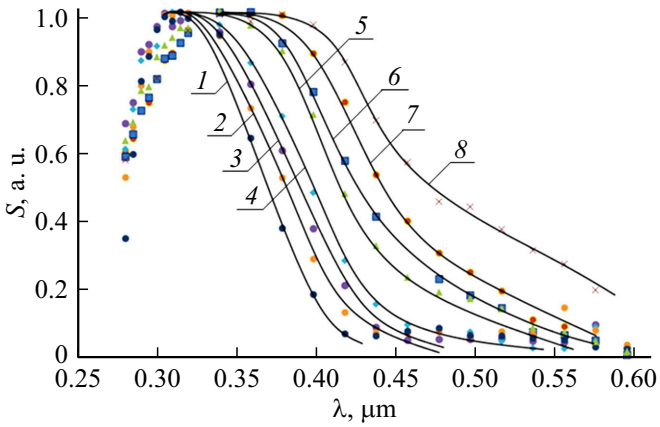

Figure 5. Spectral sensitivity of the differential channel. Alloying doses: *1* — 200, *2* — 300, *3* — 400, *4* — 500, *5* — 700, *6* — 1000, *7* — 2000, *8* — $5000\,\mu C/cm^2$.

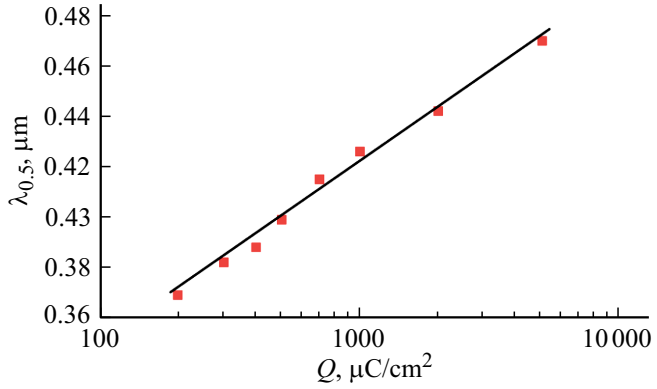

Figure 6. Dependence of the long-wavelength limit of the differential channel sensitivity on the implantation dose As.

magnitude of the implantation dose As. A series of photodetectors with different degrees of doping of the auxiliary channel [33,34] has been fabricated in this regard. The normalized spectral characteristics of differential channels for equal flux of incident quanta at different doping doses of the additional channel are shown in Fig. 5.

As might be expected, with increasing implantation dose, a broadening of the spectral range of sensitivity was observed due to a shift in the long-wavelength limit. Of interest is the experimental dependence of the long-wavelength boundary (on level $\lambda_{0.5}$) on dose of doping (Fig. 6). In the range of doses studied, it can be approximated by the expression

$$\lambda_{0.5} = \lambda_0 + k \ln \frac{Q}{Q_0},$$

where λ_0=0.347 μm, k=3.2 · 10^{-2} μm, Q_0=100 $\mu C/cm^2$.

Another important characteristic of the photodetector is the sensitivity value of the differential channel, which also depended on the doping dose of the auxiliary channel. The quantum efficiency of the differential channel for different

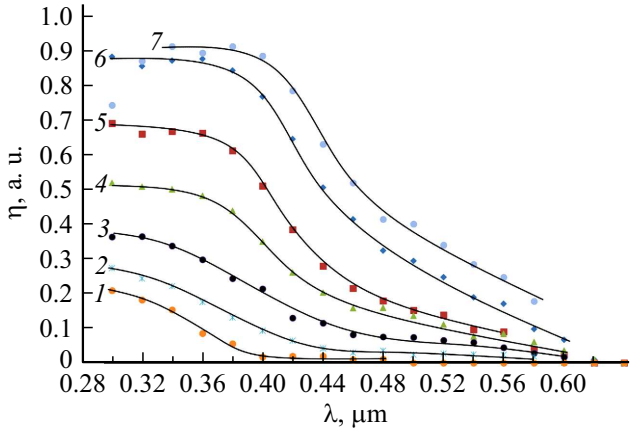

Figure 7. The quantum efficiency of the differential channel for different implantation doses As: *1* — 200, *2* — 300, *3* — 500, *4* — 700, *5* — 1000, *6* — 2000, *7* — 5000 μC/cm^2.

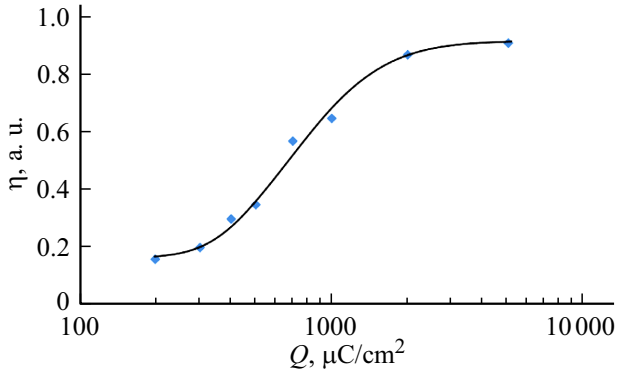

Figure 8. Dependence of differential channel quantum efficiency on implantation dose As for $\lambda = 0.34\,\mu$m.

implantation doses is shown in Fig. 7. The values are given as the ratio of the quantum efficiency of the differential channel to the maximum value of the quantum efficiency of the main channel.

An increase in differential channel signals was observed with increasing dose. Fig. 8 shows an analysis of the dependence of the differential channel efficiency on the implantation dose As for a fixed wavelength near the maximum of the spectral response $\lambda = 0.34\,\mu$m.

In the range from 200 to 2000 μC/cm^2, a significant dose effect on the sensitivity of the differential channel was observed. Starting at 2000 μC/cm^2, the value of quantum efficiency approached 90%, and further increases in dose had little effect on sensitivity. Thus, if we do not set the problem of correcting the long-wavelength boundary with respect to $\lambda_{0.5} = 0.44\,\mu$m, then close to optimal doping doses around 2000 μC/cm^2. At the same time, good selectivity of the spectral response was maintained and high sensitivity of the differential photodetector was ensured.

3. Electrical characteristics of photodetectors

An important requirement for differential photodetectors is to ensure that the electrical characteristics of the main and secondary channels are identical. The current-voltage curve (CVC) were measured using an Agilent B1500A semiconductor analyzer. A Microxact SPS-2800-TC probe rig was used for temperature measurements.

The CVC of the main and complementary channels were measured over a range of arsenic doping doses from 200 to 5000 μC/cm^2 [35]. For each CVC process series, the photodiodes of the main (*1*) and auxiliary (*2*) channels at low voltages had a similar form with no significant dependence on the doping dose of the auxiliary channel. As an example, the direct branches of the dark CVC of one of the photodetectors are shown in Fig. 9. As can be seen, in the area of small currents at voltages up to 0.5 V, an exponential dependence corresponding to the generally accepted form [36] was observed:

$$I = I_0\left[\exp\left(\frac{eU}{\beta kT}\right) - 1\right]$$

with values $I_0 \approx 1 \cdot 10^{-11}$ A, $\beta = 1.11$. At low voltages for the main and auxiliary channels, the appearance of the CVC was similar. At higher voltages, the series residual resistance of the diodes began to be affected, and the CVC went to the linear section. For some samples, as observed in the above example, a slight difference in the residual resistance values was evident in the high current area. Thus, in this case, the differential resistances were: for the main channel $R_1 = 9.4\,\Omega$ and additional $R_2 = 11.2\,\Omega$. However, it should be considered that the preferred mode for photodiode operation is the mode with zero or small negative voltages at the $p-n$-junction. At the same time, the observed difference in the area of large positive displacements is not significant. For samples of many other technological series in the direct

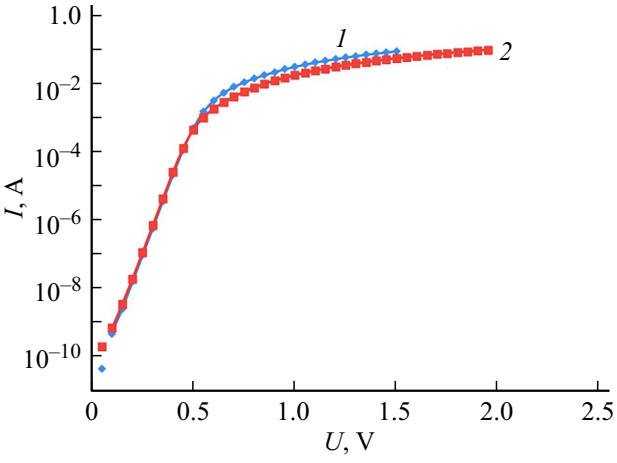

Figure 9. Straight branches CVC. Alloying dose 500 μC/cm^2: *1* — main, *2* — additional channel.

branch, almost complete coincidence of CVC up to currents of the order of 100 mA was observed.

Typical dependences of the inverse dark current are given in Fig. 10. Near breakdown voltages, at which the reverse current for the main channel increased markedly, reached 140–160 V. Given the developed cumulative length of the $p-n$-junction boundaries of the multi-plane photodiode, we can assume a significant influence of surface leakage on the reverse current character. As might be expected, the ultimate stresses were lower for the additional channel having a high concentration of structural defects in the near-surface area.

Fig. 10 also shows the initial part of the characteristic in the range of small voltages, which are of most interest in practice. The characteristics of the main and supplementary channels were similar, but numerically slightly different. As can be seen, the reverse current did not experience saturation. The magnitudes of the currents at low voltages were much larger than $I_0 \approx 10$ pA (thus, at $U = 1.6$ V, $I_1 = 107$ pA, $I_2 = 160$ pA and increased linearly with voltage. This could indicate the presence of excessive currents. The diode current at small biases can be represented by the sum of summands

$$I(U) = I_d(U) + I_{gr}(U) + G_s U,$$

where I_d, I_{gr} — diffuse and generation-recombination components of the diode current, G_s — leakage conductance.

Although V.I. Stafeev in his work [37] showed that the additivity of the ideal diode current and leakage current is not strictly fulfilled, nevertheless the above formula can be useful as reflecting the near ohmic character of the current change in the device. For quantitative characterization, leakage resistances can be estimated, which for the sample under consideration were $R_{s_1} = 14 \cdot 10^9$ and $R_{s_2} = 8.9 \cdot 10^9$ Ω. Knowledge of dynamic impedances is necessary for selecting preamplifier characteristics.

Fig. 11 shows the temperature dependence of the leakage resistance for the main channel of a photodetector with doping dose 500 μC/cm^2 in the positive temperature area from 0 to +60°C. The results can be approximated by an

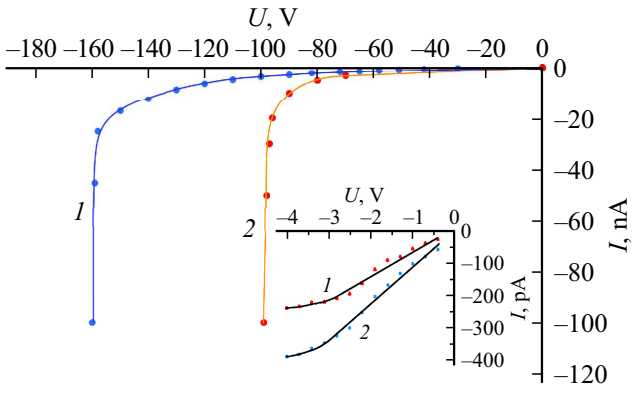

Figure 10. Reverse branches of the CVC: *1* — main channel, *2* — additional channel. Dose 500 μC/cm^2.

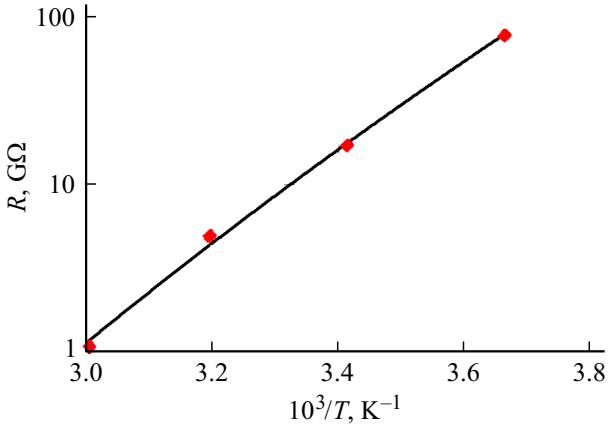

Figure 11. The dependence of leakage resistance on temperature.

exponential dependence with an activation energy close to half of the silicon band gap width (about 0.54 eV). It was many orders of magnitude higher than typical preamplifier input impedances ($R_{inp} < 10^3$ Ω). This makes it possible to ignore differences in channel leakage resistance values and reliably record the difference signal with a differential amplifier over the entire temperature range of practical interest. Changing the doping doses did not reveal any significant effect on the electrical characteristics of both main and additional channels.

The barrier capacitances for the given photodetector topology at zero bias had values of about 440 pF for the main channel and 390 pF for the auxiliary channel. The difference is due to the slightly larger metallization area of the main channel.

4. Directional diagram of the photodetector

One of the specific features of differential photodetectors became apparent in the study of their directional pattern [38]. Directional patterns were recorded with a goniometer G5 using monochromatic light sources separately for shortwave and longwave radiation. An LED with wavelength 0.402 μm was used as the short-wavelength source, and an LED with wavelength 0.625 μm was used as the long-wavelength source. The emission of the LEDs was modulated at a frequency of 1000 Hz with current amplitude values of 10 mA. This ensured the operation of photodetectors on the linear part of their energy characteristic with the level of signals significantly exceeding the noise ones. Signals were recorded at the output of the differential amplifier with a selective microvoltmeter B6-9.

The directional patterns for photodetectors using two types of packages were investigated. In the first case, the photosensitive structure was mounted in a standard metal box KT-2 housing equipped with an optical window. The directivity diagrams of both the main (wide-band) and differential channels in the short wavelength area had

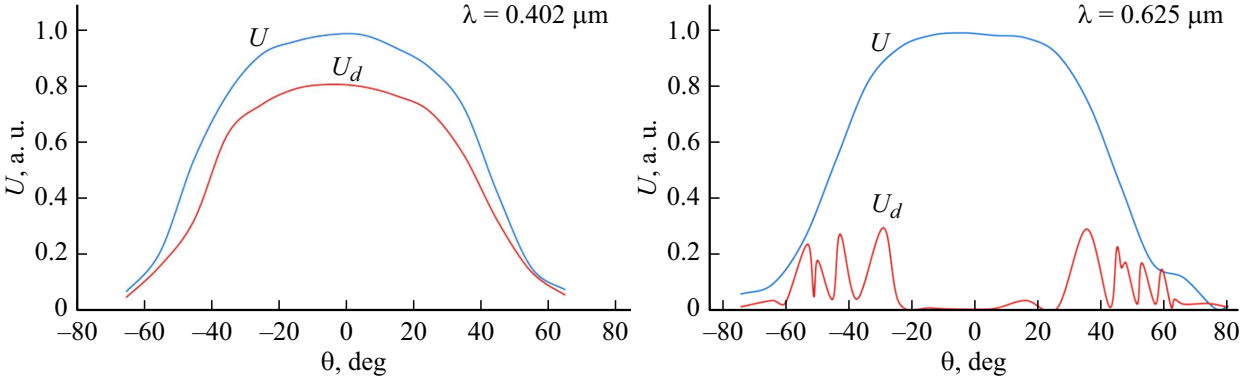

Figure 12. Directional diagrams of the main (U) and differential (U_d) channels of the first type photodetector in the shortwave ($\lambda = 0.402\,\mu$m) and longwave ($\lambda = 0.625\,\mu$m) areas.

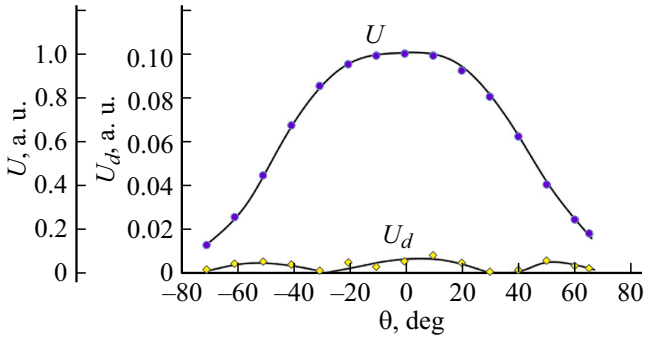

Figure 13. Directional diagram of the main (U) and differential (U_d) channels of the second type photodetector in the long-wave area ($\lambda = 0.625\,\mu$m).

a traditional form for photodetectors. The flat angle of view (2β) at level 0.5 [39] was for both the main and differential channels of $2\beta \approx 90°$. The specific feature in the directivity diagram was manifested in the long-wave area of the spectrum (Fig. 12).

The differential channel is designed to record only short-wave radiation, and its sensitivity in the long-wave area should be as low as possible. However, a number of parasitic maxima were observed for the differential channel at off-axis angles starting at angles of the order of 30°. Their appearance can be associated with partial shading of photosensitive areas by the walls of the recessed body of the photodetector, especially pronounced at the boundaries of the directivity diagram. Since the differential signal was formed by subtracting the signals of adjacent neighboring photodiodes, uneven illumination of the sites led to the edge effect and the formation of a spurious signal. To eliminate the effect, mounting of the photosensitive structure in a flat case KT-93 (second type) was used.

The directional diagram of such a photodetector for long-wave radiation is given in Fig. 13. As can be seen, the exclusion of the influence on the illumination of the photosensitive structure of the housing design elements resulted in a significant suppression of parasitic edge effects. The low level of signals of the differential channel indicated the homogeneity of illumination of sensitive sites and preservation of selectivity of the spectral response of the photodetector for all angles of the directivity diagram. Another option for eliminating edge effects may be to use a matte (scattering) input window [40].

5. Current sensitivity and threshold characteristics of the photodetector

The absolute current sensitivity values of the differential channel for monochromatic radiation (S_λ) [41] were measured. For this purpose, a UV LED with an emission peak at wavelength $0.36\,\mu$m with a spectrum half-width of $0.013\,\mu$m was used, which agreed with the maximum spectral sensitivity of the photodetector. The value of current sensitivity was determined by comparing the signals of the investigated photodetector with a known one. An FDUK-10 [42] photodiode was used as a comparison receiver. The values of current sensitivity of the differential channel for the photodetector with doping dose $2000\,\mu$C/cm^2 were $S_i = 0.06$ A/W. Calculating the current sensitivity for 100% quantum efficiency at $\lambda = 0.36\,\mu$m [43] gives a value of 0.29 A/W. Taking into account that the area of sensitive areas of the main channel was 32% of the total area of the photodetector, as well as the decrease in sensitivity due to the subtraction of signals from the auxiliary channel (in our case it is 12%), the calculated value of $S_i$is 0.082 A/W. If we also take into account the presence of additional losses on reflection of radiation by the entrance window and the structure itself, the obtained values of $S_i = 0.06$ A/W can be considered quite an acceptable result.

In some cases, it may be necessary to increase the size of the sensitive area of the photodetector. For example, to increase the sensitivity of a photodetector to illumination or to extend the field of view of a device with a given optical system. One of the advantages of the proposed photodetectors is the possibility to increase the area by connecting the modules in parallel. The required number

of modules can be assembled at the final operations of device assembly without changing the main technological operations. Fig. 14 shows the obtained dependences of current sensitivity with the increase of connected modules. As can be seen, when the total area of the receiving pads was increased by 4 times, the current sensitivity did not decrease, maintaining a constant value.

The question of threshold characteristics of photodetectors is actual at registration of weak signals. The study of the noise spectrum showed that the characteristics of the main and additional channels for all samples practically coincided and did not depend on the doping dose of the additional channel.

In the absence of background illumination, the spectral characteristics of noise currents had a classical form (Fig. 15) and could be represented as a sum of two components: flicker – noise and white noise [43]. The parameter α flicker – noise ($i_{\text{noise}} \propto 1/f^{u}$) for the studied samples had a value ranging from 0.9 to 1.1, and the frequency of the conjugation of flicker – noise and white noise was 300–350 Hz. Near zero bias, the spectral density of the white noise current had a value of about $1 \cdot 10^{-13}$ A/Hz$^{1/2}$. Since photodiodes are practically not used in modes without background illumination, measurements of the photodiode

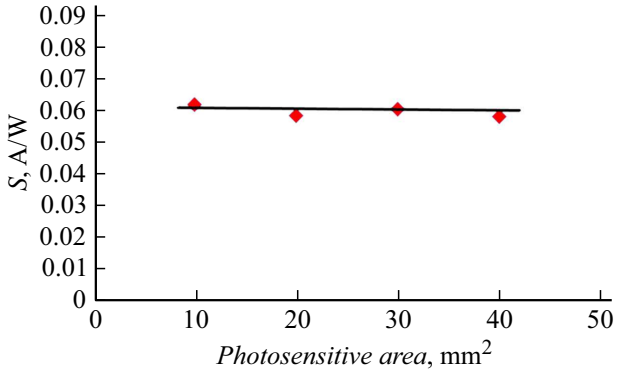

Figure 14. Current sensitivity of the differential channel for photodetectors with increased area.

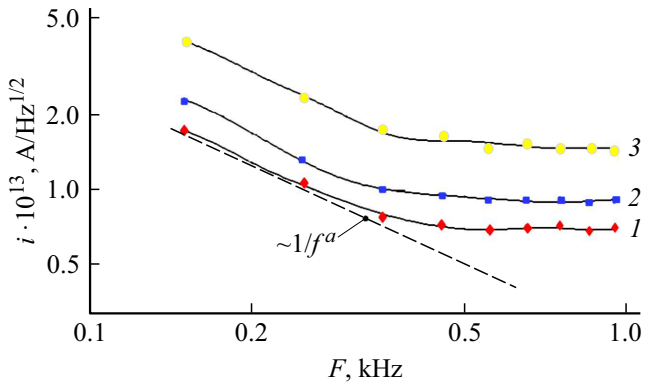

Figure 15. Spectral characteristics of the complementary channel noise current for the 500 μC/cm^2 doped dose in the absence of background illumination: U_{suppl}: *1* — 0.5, *2* — 2, *3* — 10 V.

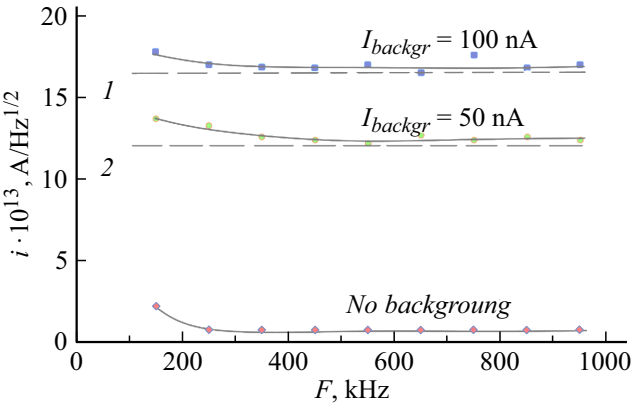

Figure 16. Spectral characteristics of the shot noise current of the complementary channel with 500 μC/cm^2 d oping dose at different background currents and supply voltage 0.5 V. *1* — theoretical value of shot noise current at $I_{backgr} = 100$ nA; *2* — theoretical value of shot noise current at $I_{backgr} = 50$ nA.

noise current when the photodiodes are exposed to background radiation flux were carried out. A stable current fed incandescent lamp was used as a background source. The background flux level was controlled by varying the lamp supply current, and monitored by the magnitude of the background current of the test sample. The measurements are shown in Fig. 16.

As can be seen, at background currents of $I_{backgr} > 50$ nA, the noise current of each channel for frequencies above 300–350 Hz was almost completely determined by the shot noise of its background current and could be determined by the Schottky [44] formula:

$$i_{\text{noise}} = \sqrt{2eI_{backgr}\Delta f},$$

where e — electron charge, I_{backgr} — phonon current, Δf — bandwidth.

Based on the data obtained, operating voltages in the range from 0 to 0.5 V can be considered optimal for both channels of the differential photodetector. According to our estimates, the noise characteristics of silicon differential photodetectors for daylight at frequencies above 350 Hz will be determined by fluctuations of background radiation starting from illuminance about 10 *lx* [45].

6. On the application of silicon differential photodetectors

The application of silicon differential photodetectors as short-wave photodetectors operating in the UV range should be considered the most demanded. At the same time, the sensitivity areas of the differential and additional channels had a pronounced shift relative to each other in the short-wave and long-wave parts of the spectrum. This allows differential photodetectors to be used as dual-color photodetectors. The spectral characteristics of the photodetector with the widest spectrum of the differential

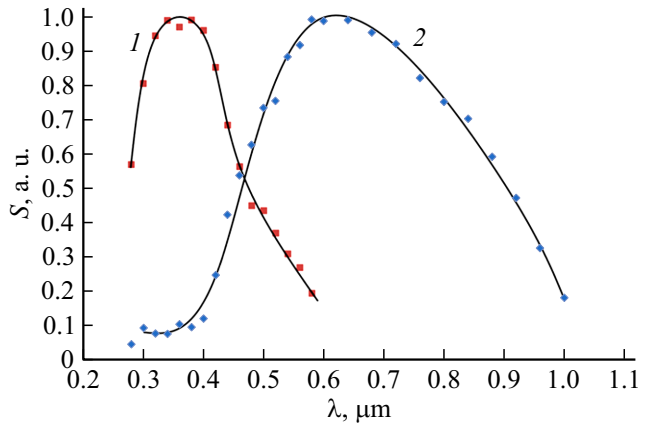

Figure 17. Spectral characteristics of differential (*1*) and complementary (*2*) channels.

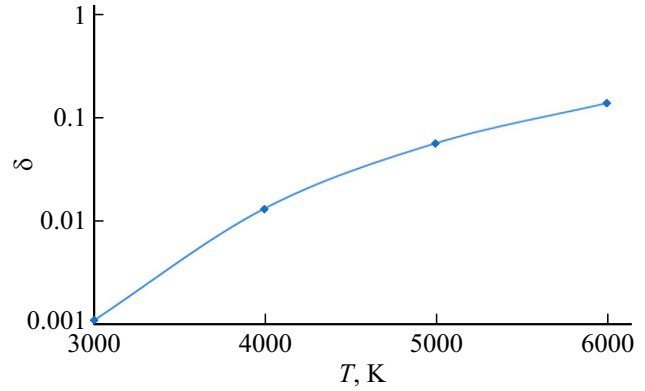

Figure 18. Dependence of the ratio of signals of the differential channel to the complementary channel on the temperature of the heat source.

channel (doping dose $5000\,\mu C/cm^2$) are shown in Fig. 17. As can be seen, the sensitivity maxima were in the UV region ($\lambda_{max} = 0.37\,\mu m$) for one channel and in the visible region ($\lambda_{max} = 0.6\,\mu m$) for the second channel. The possibility to register optical radiation simultaneously in two separated spectral ranges may be of practical interest, as it allows for prompt spectro-zonal analysis of emitting objects. The relevance of the development of multispectral optoelectronic systems (OES), in which one of the spectral channels would have sensitivity to radiation in the UV spectral range, and the other channel — in the visible or IR area of the spectrum, is associated with the possibility of their application in such areas as space research, nanolithography, military technology, medicine, monitoring, emergency etc. [46,47].

As an example, we can consider the use of such a photodetector to determine the temperature of thermal radiation sources. Fig. 18 shows the calculated dependence of the ratio of the signals of the differential and additional channels ($\delta = U_{dif}/U_2$) on the temperature of the heat source.

The ratio of differential channel signals to longwave signals for different light sources

No.	Light source	Ratio signals δ, a.u.
1	Incandescent lamp, 75 W	0.0025
2	LED bulb, warm color, 10 W (LEDGSLE27)	0.186
3	Fluorescent lamp, warm color, 30 W (CF30-ASE27)	0.212
4	LED bulb, cold color, 17 W (LED-17 A65/865/E27)	0.247
5	LED bulb, cold color, 7 W (17FQ)	0.283
6	Fluorescent lamp, cold color, 15 W	0.304

The data are obtained by numerical integration method. As a model of the radiation source, the ACT with the character of photon flux distribution is assumed to be [48]:

$$N_\lambda = \frac{2\pi c\lambda^{-4}}{\exp\frac{C_2}{\lambda T} - 1},$$

where N_λ — number of photons emitted in all directions from a unit area in a unit frequency range, c — the speed of light, λ — wavelength, T — temperature, $C_2 = 1.44\,cm \cdot K$.

The signal ratio was calculated as

$$\delta = \frac{\Sigma_i N_{\lambda_i}\eta_{\lambda_1}}{\Sigma_i N_{\lambda_i}\eta_{\lambda_2}},$$

where $\eta_{\lambda_1}, \eta_{\lambda_2}$ — relative channel quantum efficiencies *1* and *2*. Summation was performed in increments of $0.02\,\mu m$. As can be seen, when the temperature decreases from 6000 K (solar radiation) to 3000 K (incandescent lamp), the signal ratio should change significantly, decreasing by two orders of magnitude. This makes it possible to use such photodetectors for monitoring high-temperature radiation sources and for effective analysis of the type of radiation sources — for example, in fire detectors to avoid false alarms by recognizing the difference between the spectrum of solar glare and the spectrum of thermal radiation from fire sources. A photodetector with the widest possible differential channel spectrum (dose $5000\,\mu C/cm^2$) was chosen as the model most suitable for such an application.

Another interesting application of the dual-spectral photodetector is its use for testing light sources. Many modern sources utilize the conversion of UV radiation to visible light. The presence of a significant proportion of UV radiation in household light sources is highly undesirable [49]. The need to improve the devices and methods for assessing the quality of light sources is

considered to be an urgent task [50]. In our opinion, silicon differential photodetectors can be used for these purposes [51]. The table shows examples of measuring the ratio of differential channel signals to longwave ($\delta = U_d/U_2$) for some light sources. The doping dose of the additional channel was $2000\,\mu C/cm^2$. As can be seen, there was a significant variation in the value of δ for different light sources. It should also be noted that, in addition to spectroscopic analysis, differential photodetectors allow measuring the level of intensity ripples, which is also a relevant characteristic of artificial light sources [52]. An additional advantage of such photodetectors is the possibility to analyze pulsations separately for both UV and visible components of the spectral range.

Conclusion

The possibilities of application of differential methods of signal registration of silicon photodetectors for controlling the range of spectral sensitivity are considered. To improve the homogeneity of the characteristics, it is proposed to form the channels as two groups of parallel photodiodes staggered in parallel. The experimental dependence of the long-wavelength limit of the differential signals on the implantation dose As is presented. The recommended optimal implantation dose — about $2000\,\mu C/cm^2$. The study of the electrical characteristics of the main and additional channels showed the possibility of reliable registration of the difference signal with the help of a differential amplifier in the whole temperature range of practical interest. Deep enclosures are not recommended to avoid parasitic signals when radiating laterally. The measured differential channel current sensitivity values for the photodetector with $2000\,\mu C/cm^2$ doping dose were $S_i = 0.06$ A/W at the $0.36\,\mu m$ wavelength. One of the advantages of the proposed photodetectors is the possibility to increase the receiving area within wide limits due to the parallel inclusion of modules. Examination of the noise spectrum showed that near zero bias at frequencies above 300−350 Hz for the dark current, the white noise spectral density had a value of about $1 \cdot 10^{-13}$ A/Hz$^{1/2}$. Besides the application of silicon differential photodetectors as short-wave photodetectors operating in the UV range, it is possible to use them as two-color photodetectors, for example, for remote analysis of radiation from high-temperature thermal sources or as quality testers of artificial light sources.

Funding

The research was supported by the Ministry of Education and Science of the Russian Federation within the basic part of the state task, project №1755.

Conflict of interest

The authors declare that they have no conflict of interest.

References

[1] A.M. Prokhorov (Editor-in-Chief) *Fizicheskiy entsiklopedicheskiy slovar* /Gl. red. A.M. Prokhorov (Sovetskaya entsiklopediya, M., 1983) (in Russian).
[2] J. Fryden. *Modern sensors. Handbook* (Technosphere, M., 2005).
[3] N.T. Gurin, S.G. Novikov, I.V. Korneev, A.A. Shtanko, V.A. Rodionov. Pisma v ZhTF **37**, (6), 57 (2011). (in Russian).
[4] M.V. Kitaeva, A.V. Yurchenko, A.V. Ohorzina, A.V. Skorokhodov. Polzunovskij vestnik, **3/1**, 196 (2011) (in Russian).
[5] A.M. Filachev, V.P. Ponomarenko, I.I. Taubkin. Prikladnaya fizika, **2**, 102 (2003). (in Russian).
[6] M.L. Baranochnikov. *Priyemniki i detektory izlucheniy.. Spravochnik* (DMK Press, M. 2012)
[7] I.D. Anisimov, I.M. Vikulin, F.A. Zaitov, Sh.D. Kurmashev. *Poluprovodnikovyye fotopriyemniki: Ul'trafioletovyy, vidimyy i blizhniy IK diapazony spektra* (Radio i svyaz', M., 1984)
[8] R.J. Kies (ed.). *Fotopriyemniki vidimogo i IK diapazonov*. Transl. from English. (Radio i svyaz, M., 1985) (in Russian).
[9] A.M. Filachev, I.I. Taubkin, M.A. Trishenkov. *Sovremennoye sostoyaniye i magistral'nyye napravleniya razvitiya tverdotel'noy fotoelektroniki* (Fizmatkniga, M., 2010) (in Russian).
[10] A.V. Voytsekhovsky, N.A. Kulchitsky, A.A. Melnikov, S.N. Nesmelov, S.M. Dzyadukh. Nano i mikrosistemnaya tekhnika,**143** (6), 30 (2012) (in Russian).
[11] Y.I. Belousov, E.S. Postnikov.*Infrakrasnaya fotonika. Chast' II Osobennosti registratsii i analiza teplovykh poley.* Manual (ITMO University, SPb, 2019).
[12] R. Hayman. *Svetofiltry*. Transl. from English. (In Russian) (Mir, M., 1988) (in Russian).
[13] E. Ritter. Fizika tonkikh plenok, **8**, 7 (1978).
[14] G.V. Rosenberg. *Optika tonkosloynykh pokrytiy* (Nauka, M., 1991).
[15] Electronic resource 0AO „LLS". Available at: info@lenlasers.ru
[16] Y.A. Goltberg, B.V. Tsarenkov. ZhTF, **66** (8), 195 (1996) (in Russian).
[17] Y.A. Glebov, N.Y. Zvereva, Y.A. Kazarova, O.G. Revzina, L.S. Shenderovich. Prikladnaya fizika, **3**, 84 (2007). (in Russian).
[18] Sh.A. Furman. *Tonkosloinye opticheskie pokrytiya* (Mashinostroenie, L., 1977) (in Russian).
[19] G.Ya. Kolodny, E.A. Levchuk, Y.D. Poryadin, P.P. Yakovlev. Elektron. Prom-st., **5**, 93 (1981). (in Russian).
[20] V.V. Gavrushko, A.S. Ionov, V.A. Lastkin. Nauka, Tekhnologiya, Biznes, **100** (2), 72 (2010). (in Russian)
[21] US Patent №7196311, H01L 27/15 dated 11.08.2005.
[22] BY Patent №8532 U1, H01L 27/15 dated 30.08.2012.
[23] Patent RU №156627 U, H01L 31/068 dated 05.05.2015.
[24] V.V. Gavrushko, A.S. Ionov, O.R. Kadriev, V.A. Lastkin. ZhTF, **87** (2), 310 (2017). (in Russian)
[25] R. Korde, L.R. Canfield, B. Wallis. Proc. SPIE, **932**, 153 (1988).
[26] V.V. Gavrushko, A.S. Ionov, V.A. Lastkin. Datchiki i sistemy, **121** (6), 49 (2009).
[27] V.V. Gavrushko, V.A. Lastkin. Vestnik of Novgorodskogo gos. un-ta, **65**, 17 (2011). (In Russian)

[28] V.V. Gavrushko, A.S. Ionov, V.A. Lastkin. *Tez. dokl. IV Vserossiyskoy konferentsii „Fizicheskiye i fiziko-khimicheskiye osnovy ionnoy implantatsii"* (Novosibirsk, Russia, 2012), p. 37.
[29] A.P. Gorshkov, I.A. Karpovich, E.D. Pavlova, N.S. Volkova. FTP, **46** (12), 1542 (2012) (in Russian).
[30] S. Namba. *Technology of Ion Doping*. Per. s Japanese (Sov. Radio, M., 1974)
[31] V.S. Vavilov, A.R. Chelyadinskiy. UFN, **165** (3), 347 (1995) (in Russian).
[32] J.F. Ziegler, J.P. Biersack, M.D. Ziegler. Nucl. Instrum. Methods Phys. Res. B, **268**, 1818 (2010).
[33] V.V. Gavrushko, A.S. Ionov, V.A. Lastkin.*Patent na poleznuyu model' kremniyevyy fotopriyemnik s zadavayemoy spektral'noy kharakteristikoy*(№166199 27.11.2016)
[34] V.V. Gavrushko, A.S. Ionov, O.R. Kadriev. Mater. Sci. Eng., **441** (1), 1 (2018).
[35] V.V. Gavrushko, A.S. Ionov, O.R. Kadriev, V.A. Lastkin. J. Phys.: Conf. Series, **2052**, 012 (2021).
[36] V.V. Pasynkov, L.K. Chirkin, A.D. Shinkov. *Poluprovodnikovye pribory* (M., Vyssh. shk., 1981) (Russian).
[37] V.I. Stafeev. FTT, **3**, (1), 185 (1961). (in Russian).
[38] V.V. Gavrushko, O.R. Kadriev, V.A. Lastkin, A.A. Sapozhnikov. Vestnik of Novgorodskogo gos. un-ta, **104** (6), 17 (2017). (In Russian)
[39] GOST 21934-83 *Priyemniki izlucheniya poluprovodnikovyye fotoelektricheskiye i fotopriyemnyye ustroystva.*
[40] Patent RU № 1763331 U1, H01L 31/068 dated 02.05.2017
[41] V.V. Gavrushko, A.S. Ionov, O.R. Kadriev, V.A. Lastkin. Vestnik of Novgorodskogo gos. un-ta, **107**, 4 (2018). (In Russian)
[42] V.V. Zabrodsky, P.N. Aruev, V.P. Belik, B.Ya. Ber, D.Yu. Kazantsev, M.V. Drozdova, N.V. Zabrodskaya, M.S. Lazeeva, A.D. Nikolenko, V.L. Sukhanov, V.V. Philimonov, E.V. Sherstnev. FTP, **47**, (2), 178 (2013). (in Russian).
[43] A.V. Klyuev, E.I. Shmelev, A.V. Yakimov. Izvestiya Vuzov. Radiofizika, **LVII** (12), 995 (2014). (in Russian).
[44] S. Zi. *Fizika poluprovodnikovyk priborov* (M., Mir, 1984) v. 2. (in Russian).
[45] V.V. Gavrushko, A.S. Ionov, A.A. Sapozhnikov. Vestnik of Novgorodskogo gos. un-ta, **109** (3), 13 (2018). (In Russian)
[46] M.A. Trishenkov. *Fotopriyemnyye ustroystva i PZS. Obnaruzheniye slabykh opticheskikh signalov* (Radio i svyaz'., M., 1992)
[47] V.I. Sankin, V.P. Chelibanov. Phys. Stat. Sol. A, **185** (1), 153 (2001).
[48] I.K. Kikoin, (red.) *Tablitsa fizicheskikh velichin. Spravochnik* (Atomizdat, M., 1976) (in Russian)
[49] V.A. Kaptsov, V.N. Deinego. Health Risk Analysis, **13** (1), 15 (2016).
[50] A. V. Vinogradova, M. R. Sidorova. *Expertiza. Kachestvo. Tekhnologii. Sb. mater. Mezhdunar. scientific-practical conf.* (Novosibirsk, 2020), p. 229 – 233.
[51] V.V. Gavrushko, O.R. Kadriev. Vestnik of Novgorod State University named after Yaroslav the Wise, **2** (114), 4 (2019).
[52] V.N. Krasnoshchekova, N.V. Ilyukhin, S.S. Romanova, L.H. Akhmetova. Gigiyena truda i meditsinskaya ekologiya, **3**, 98 (2015).

Translated by Y.Deineka